An experimental power pick-up mechanism for an electrically driven UAV.

D I Jones
GWEFR Cyf
Pant Hywel, Penisarwaun,
Caernarfon, Gwynedd LL55 3PG,
Wales

formerly with:
School of Electronic Engineering
University of Wales,
Bangor, Gwynedd LL57 1UT,
Wales

***Abstract*— An actively controlled mechanism for picking up electrical power from the conductors of an overhead line on a distribution network is described. The mechanism is part of a novel concept for inspecting power lines from an unmanned aerial vehicle (UAV). The background to the application is explained and an outline given of a small, ducted-fan rotorcraft which draws its power from the overhead line (OHL). A cranked linkage is proposed that maintains a firm sliding electrical contact with the OHL and compensates for the movement of the rotorcraft. The paper contains details of a kinematic analysis and 3D computer visualization of the mechanism's working range. The design of an experimental pick-up mechanism is described and a computer simulation shows how impedance control can regulate the contact force with the OHL. Experimental results using an Air Vehicle Simulator (AVS) are presented to verify the action of the pick-up mechanism.**

I. INTRODUCTION

Inspection of power lines on distribution networks is an important potential civil application for unmanned aerial vehicles (UAVs). The role of the UAV is to transport a sensor package along the overhead line. The primary sensors are video cameras whose imagery can be analysed for the purpose of asset management [1], [2] but could also include other sensor types [3]. A new concept for this purpose has recently been proposed [4] based on a small, electrically-driven rotorcraft operating close to the overhead line and obtaining its power directly from the conductors, as illustrated in Fig. 1. One part of the feasibility study for this concept has considered how a pick-up mechanism could be fixed to the vehicle and actively regulated to maintain contact with the overhead line despite changes in position and attitude caused by wind gusts.

The proposed air vehicle is of the 'ducted-fan' type. Several of these now exist, such as the BAE Systems IAV2 and Bertin Technologies' HoverEye. This configuration has several advantages over a free-flying helicopter. The ducted fan is efficient at hover and at the low speeds required for inspection. The duct gives protection from the propellers if a fault condition causes it to fall to the ground. The electrical drive means that no fuel is carried, so there is no risk of serious fire in the case of an accident. Obtaining power from the overhead line allows the vehicle to be used for long missions and the electrical drive is quieter than an internal combustion engine. Working close to the overhead line gives good inspection detail and may even allow some measurements which require physical contact to be made.

A crucial feature of this concept is that only limited on-board battery power is available, effectively tethering the vehicle to the immediate vicinity of the line. Even under the worst-case fault condition of its control system demanding maximum altitude, it cannot pose a hazard to other aircraft as it does not have an on-board energy source to maintain free flight. This is an important factor in preparing a safety case for operation outside visual range of the operator. Civil liberties groups will also be re-assured by the knowledge that the vehicle's surveillance capability is restricted to the immediate vicinity of the power lines.

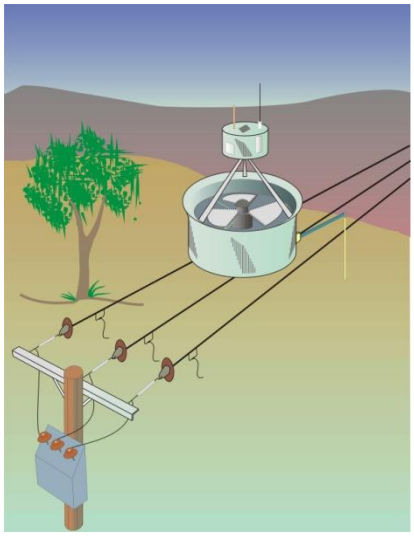

Fig. 1 Artist's impression of the power line inspection UAV.

Collecting power requires a firm sliding electrical contact between the air vehicle and the overhead line conductors. The paper describes the physical configuration of the proposed pick-up mechanism and the construction of a 1/5th scale experimental version. Computer simulation is used to show that impedance control is an effective method for adjusting the pick-up arm to maintain the required contact. This is confirmed by measurement on the experimental mechanism. Finally, the results of tests using an Air Vehicle Simulator (AVS) are presented which demonstrate the feasibility of the idea.

II. MECHANICAL DESIGN

A. Physical configuration

A typical 3-phase overhead network has bare conductors of stranded copper or aluminium steel core of 25-50 mm^2 cross-section supported on porcelain insulators fixed to wood poles. They operate at 11KV rms line voltage and have conductor spacing in the range 0.75 – 0.95m. Lightly loaded spur lines may carry less than 1A of current while a heavily loaded main line might carry around 200A. Although the vehicle's primary motion is along the line, the pick-up mechanism must compensate for perturbations in all six degrees of freedom caused by random wind gusting, ensuring that an almost constant contact force is exerted on the conductors. When obstacles are encountered (such as the in-line insulators illustrated in Fig. 1) a brief period of free flight is necessary, relying on internal battery power until contact with the lines is re-established. This requires the pick-up mechanism to be retractable.

The initial proposal was to use an inverted version of a conventional railway type pantograph, consisting of a pick-up bar suspended from a hinge beneath the air vehicle and carrying three brushes which rested on the conductors. However, this arrangement is not well suited for compensating the lateral displacement of the air vehicle with respect to the conductors. Further, overhead lines conductors have slightly different heights and spacings, which would require the brush positions to be separately adjustable. Instead, a novel arrangement of two cranked links is proposed, which can make contact with the sides of the two outer conductors. This is illustrated in Fig. 2, where the horizontal suspension bar is rigidly fixed to the bottom of the air vehicle (not shown) and has a nominal length equal to the separation of the outer conductors. Using a servo to control the angles of the two links allows this configuration to compensate for all six degrees of freedom of vehicle motion.

A 3D model was constructed in Matlab to help visualize the required link angles as the suspension bar changes in position and orientation with respect to the OHL. The shapes of the post and OHL are specified in the World reference frame {W}, as shown in Fig. 3. The contact rod shape is specified in {R}, then transformed to the aircraft reference frame {A} through the link angles θ and ψ and finally to {W} through ZYX Euler angles fixed in {A}, using the homogeneous transformation matrix ${}^{W}_{R}R$.

B. Kinematic analysis

It is of interest to know what the link angles θ and ψ should be in order that contact with the OHL is maintained as the position and orientation of the suspension bar change. From Fig. 3, this requires the point of intersection between the contact rod and its associated OHL to be calculated. If the OHL is assumed to be locally straight (instead of a catenary) then the condition for intersection of two lines in 3D space whose parametric equations are:

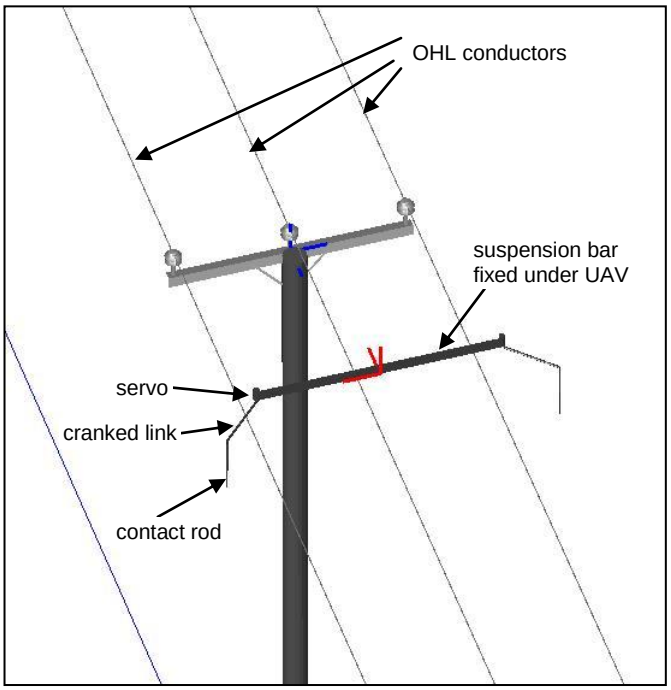

Fig. 2. Output of a Matlab 3D visualization program showing the pick-up mechanism relative to the OHL.

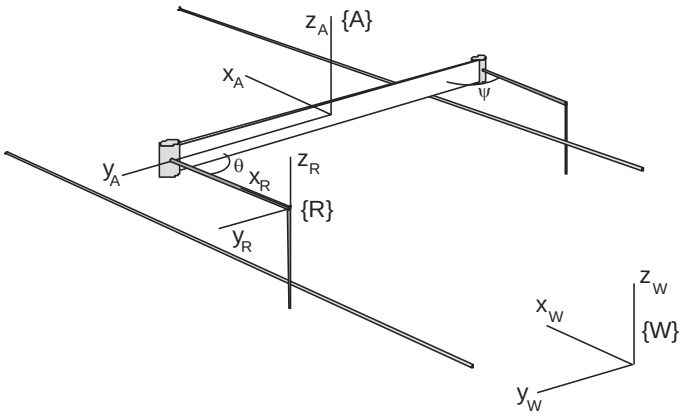

Fig. 3. Frames of reference for the 3D visualization program.

$$\frac{x - x_i}{\ell_i} = \frac{y - y_i}{m_i} = \frac{z - z_i}{n_i} = r_i \quad i = 1,2 \tag{1}$$

is given by:

$$\begin{vmatrix} x_1 - x_2 & \ell_1 & \ell_2 \\ y_1 - y_2 & m_1 & m_2 \\ z_1 - z_2 & n_1 & n_2 \end{vmatrix} = 0 \tag{2}$$

where (x_i, y_i, z_i) are points on the lines of length r_i and direction cosines (ℓ_i, m_i, n_i), expressed in {W}. The OHL conductor (i = 1) can be regarded as a line at a known position (x_1, y_1, z_1) that is parallel to x_W (so that $\ell_1 = 1$, $m_1 = 0$, $n_1 = 0$).

The contact rod (i = 2) is a line segment co-linear to z_R. Substituting in (2) gives the necessary intersection condition:

$$m_2(z_1 - z_2) = n_2(y_1 - y_2) \qquad (3)$$

where the co-factor of $(x_1 - x_2)$ vanishes because it is immaterial at what point along the line the contact occurs. The terms m_2, n_2, y_2 and z_2 in (3) are functions of the link angle θ.

If $[\hat{X}_R, \hat{Y}_R, \hat{Z}_R]$ are the unit vectors on {R} then the homogeneous transformation matrix can be written [5]:

$$ {}^{W}_{R}R = \begin{bmatrix} : & : & : & x_2 \\ {}^{W}\hat{X}_R & {}^{W}\hat{Y}_R & {}^{W}\hat{Z}_R & y_2 \\ : & : & : & z_2 \\ 0 & 0 & 0 & 1 \end{bmatrix} \qquad (4)$$

where $[{}^{W}\hat{X}_R, {}^{W}\hat{Y}_R, {}^{W}\hat{Z}_R]$ are the direction cosines referred to {W} and (x_2, y_2, z_2) are the co-ordinates of the origin of {R} expressed in {W}. Symbolic expressions for (x_2, y_2, z_2) and ${}^{W}\hat{Z}_R = [\ell_2, m_2, n_2]$ can be obtained from (4). When substituted into (3), the cos(θ) and sin(θ) terms can be separated out to give an equation of the form:

$$A\sin(\theta) + B\cos(\theta) + C = 0 \qquad (5)$$

where the coefficients A, B and C depend on the displacement and orientation of the suspension bar. Finally, (5) can be solved for the value of θ required for intersection:

$$\theta = a\tan 2\left(-\frac{B}{A}\frac{(BC + A\sqrt{(A^2 + B^2 + C^2)})}{A^2 + B^2} + C, \; \frac{BC + A\sqrt{(A^2 + B^2 + C^2)}}{A^2 + B^2} \right) \qquad (6)$$

Angles calculated from (6) are valid if θ is real (otherwise no intersection is possible) and within the range ±π/2 (otherwise the contact rod moves ahead of the suspension bar). A test is then applied to confirm that the intersection point lies within the bounds of the line segment representing the rod. Both θ and ψ must satisfy these contact conditions simultaneously for the pick-up to establish an electrical circuit. Fig. 4 shows the configuration when the suspension has been displaced along y_A and rotated in yaw by 30° with respect to the OHL but with zero roll. The left-hand link easily makes contact with the conductor but the right-hand link must set a large angle to compensate the movement.

This procedure is used to calculate the required link angles as both lateral displacement (y) and yaw angle (α) of the suspension bar vary. At each (y, α) combination the valid range is calculated as a function of the suspension bar's roll angle (γ). The vertical bars in Fig. 5 are a 'configuration space' of valid ranges of θ, where the central dots represent the zero roll cases. Two main trends are clear : as the lateral displacement changes, the required link angle varies from –π/2 to π/2 and as the yaw angle changes an arc of valid link angles is formed. Note that the valid ranges of θ rarely exceed 20° as roll angle varies, because roll and link angle are only loosely coupled.

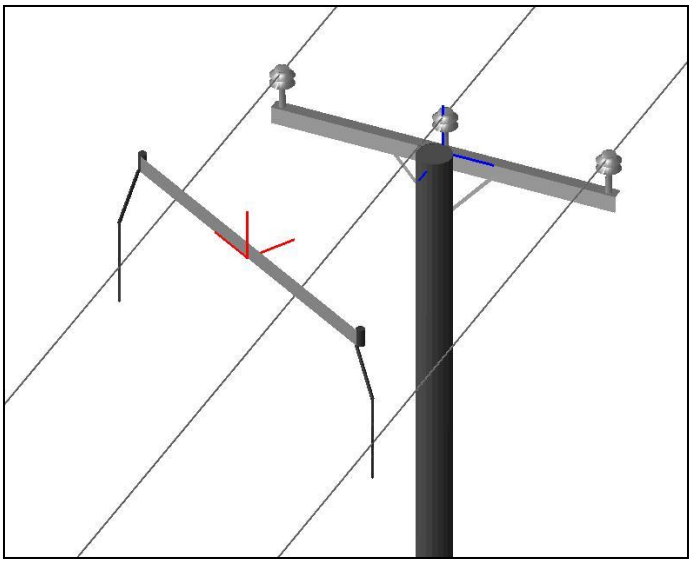

Fig. 4 Example of pick-up mechanism configuration to compensate for simultaneous yaw and lateral displacement of the suspension.

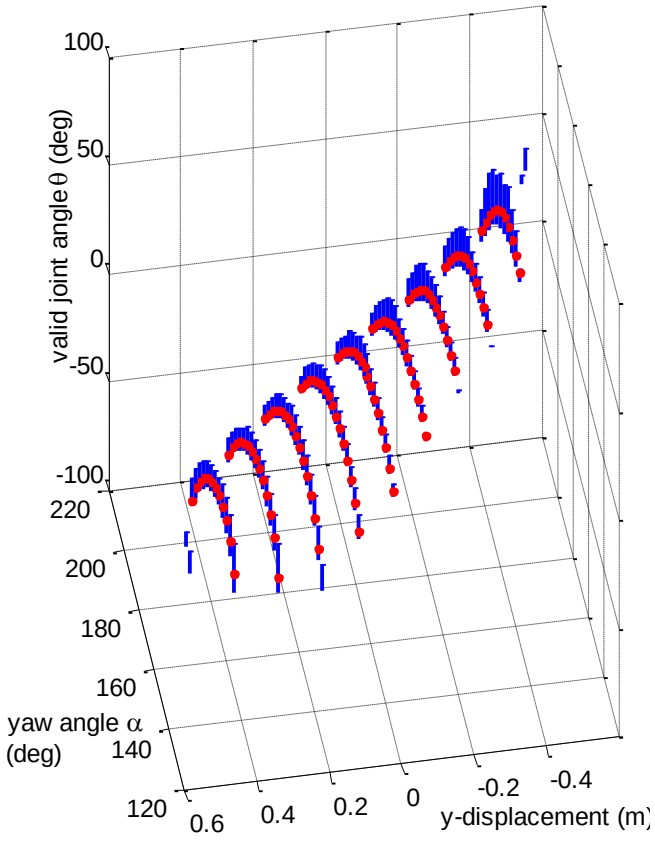

Fig. 5 Ranges of valid joint angle (θ) as a function of roll angle, yaw angle and lateral displacement.

Roll is mainly compensated for by the rod sliding on the OHL and the valid range limited by the length of the rod. It should be noted that Fig. 5 gives the ranges of possible angles but, in practice, a useful normal force could only be exerted on the conductor over the middle part of the range.

III. EXPERIMENTAL PICK-UP MECHANISM

A. *The AVS hybrid test facility*

The Air Vehicle Simulator (AVS) [6] is a hybrid test facility consisting of a four wire cable-array robot with a workspace approximately 10m long, 8m wide and 6m high. Four winches are used to adjust the cable lengths to position a simulated vehicle within the workspace.

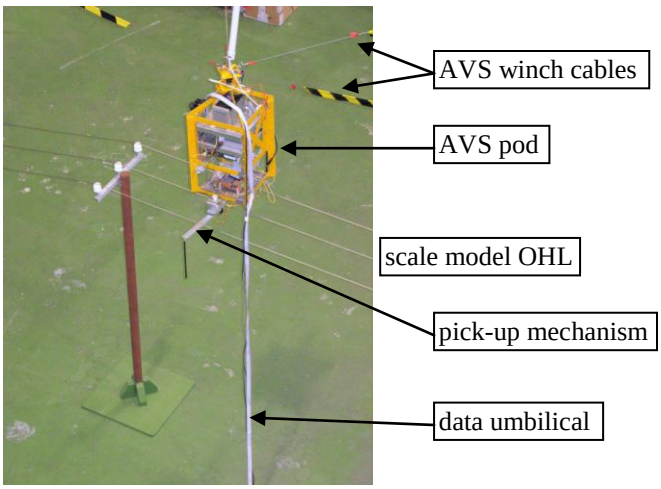

Fig. 6 Photograph of the AVS pod 'flying' above the model power lines; the experimental pick-up mechanism is fixed underneath, with links retracted.

As shown in Fig. 6, the 'vehicle' consists of a pod suspended at the conjunction of the cables, which houses a 'flight' computer, video cameras, inertial measurement unit and battery power pack. Low-level control of the winch drives is done by 4 HC12 micro-controllers, receiving demanded cable lengths from a central computer via CAN bus. The cable lengths are measured incrementally by encoders on the winch motors, with a potentiometer for calibration to absolute position. The central computer calculates the inverse kinematics, i.e. the cable lengths required for a given Cartesian pod position, which are needed to produce a programmed motion profile of the pod.

B. *Construction*

A 1/5th scale model of the pick-up mechanism was constructed, to match the dimensions of the model power lines erected in the AVS workspace. This is shown in Fig. 7. The link is made of a 180mm long brass bar of rectangular cross-section so that it is compliant orthogonal to the plane of the bar and contact rod but relatively stiff in the plane. The contact rod is a 200mm hollow aluminum/carbon tube, which is light and rigid. The brass bar is attached at the joint end to both a rigid arm, which provides protective cover, and the shaft of the servo. A force sensor is made by attaching a small bar magnet to the tip of the arm and a magnetic displacement sensor to the tip of the compliant brass bar. The stiffness at the tip is 108 N/m with a maximum displacement of ±5mm. The servo consists of a dc motor with a 84 : 1 planetary gearbox and 5:1 timing belt drive. A potentiometer measures the link angle.

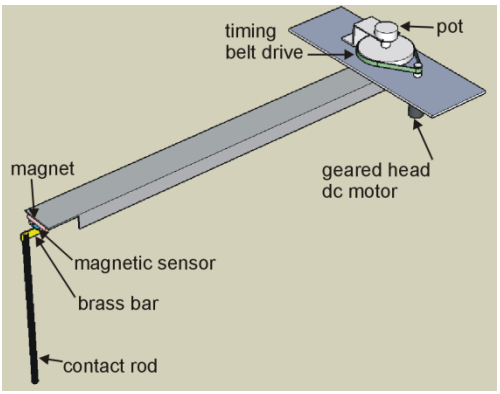

Fig. 7 Construction of the pick-up mechanism.

C. *Controller*

The purpose of the controller is to deploy the pick-up mechanism from its retracted position (-π/2) at a constant angular rate until it contacts the OHL and then maintain constant force. Impedance control [7] was chosen because it is simple to implement and uses a single control algorithm for both the free and contact phases of operation. Strictly, impedance control is not needed here because both the pick-up and OHL are compliant and the link dynamics vary little because the servo is heavily geared. Nevertheless, the method provides a useful way of addressing the control problem. Let the dynamics of the mechanism be described by [5]:

$$H(q)\ddot{q} + h(q,\dot{q}) = \tau + J^T F_c \qquad (7)$$

where q is the joint displacement vector, H(q) is the inertia matrix, h is the centrifugal, Coriolis and gravity matrix, τ is the joint torque/force vector, J is the Jacobian relating joint velocity to tip velocity and F_c is the contact force. The desired tip impedance is specified as:

$$F_c = -K(x_o - x) - B(\dot{x}_o - \dot{x}) + M\ddot{x} \qquad (8)$$

where x_o is the demanded position of the tip, x is its actual position and K, B and M are parameters chosen to specify the desired impedance. Expressing (8) as a transfer function with $\dot{x} = \ell\dot{\theta}$ and the value of K set to zero because a 'spring' action is not required:

$$\dot{\theta} = \frac{1/M\ell}{\left(s + \frac{B}{M}\right)} F_c + \frac{B/M}{\left(s + \frac{B}{M}\right)} \dot{\theta}_o \qquad (9)$$

From (9) it is clear that:

(i) $\dot{\theta}_o$ specifies the mechanism's deployment rate;

(ii) During contact, $\dot{\theta} = 0$ so $F_c = -B\dot{\theta}_o$ and B specifies the desired (constant) contact force;

(iii) For $\dot{\theta}_o$ and B fixed, M specifies the time constant of the response; reducing M increases the gain and reduces the difference between the actual contact force and the desired constant value.

The general expression for the computed torque that realizes the impedance control law is given by:

$$\tau = -J^T F_c + h(q,\dot{q}) + H(q)J^{-1}\left(M^{-1}\{K(x_o - L(q)) + B(\dot{x}_o - J(\dot{q}) + F_c\} - \dot{J}\dot{q}\right) \quad (10)$$

where L(q) is the mechanism's forward kinematics.

For a single link consisting of a distal mass m on a rod of length ℓ and a contact force normal to the tip, (9) reduces to:

$$\tau = -F_{cn}\ell(1 - \frac{m}{M}) + \frac{m}{M}\ell^2\{K\sin(\theta_o - \theta) + B(\dot{\theta}_o - \dot{\theta})\} \quad (11)$$

where, for a link of stiffness K_s:

$$F_{cn} = -K_s \ell \sin\theta \quad (12)$$

Specifying $\dot{\theta}_o = \pi/2$ and $F_c = 0.4N$, equations (11) and (12) were applied to control a single link of inertia $1/m\ell^2$. It was found that the ratio m/M = 70 gave a fast, well-damped contact transient with the located at OHL at θ = 0. This acts as the 'prototype' for the complex simulation and real-time controller in the following sections.

IV. COMPUTER SIMULATION

The computer simulation includes the dynamics of the brass rod, the OHL and the servo as shown in Fig. 8. Parameter values were obtained by measurement, from data sheets or empirically as appropriate. Velocity is estimated as a filtered derivative of the potentiometer signal. A switch selects 'contact' or 'retracted' modes, the latter being implemented as a simple proportional controller on the link angle.

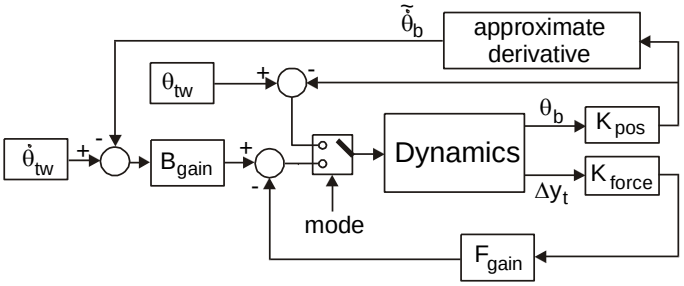

Fig. 8 Block diagram of the computer simulation.

Given that:

y_t is the position of the tip relative to the link
y_{tw} is the position of the tip in {W}
y_s is the position of the suspension in {W}
y_o is the position of the OHL in {W}
θ_t is the angle of the tip relative to the link
θ_b is the angle of the link relative to the suspension
$\Delta y_t = \ell(\theta_b - \theta_t)$ is the tip deflection
F_c is the contact force
F_t is the reaction force on the tip

then the equations for the Dynamics block in Fig. 8 are:

servo

$$n\ddot{\theta}_b = \frac{1}{J_m}\left\{\frac{\rho K_\phi}{R}\left(V - K_\phi n\dot{\theta}_b\right) - K_v n\dot{\theta}_b - \frac{\ell}{n}F_t\right\}$$

sensor (brass) bar

$$\ell\ddot{\theta}_t = \frac{1}{m_e}(F_t - F_c)$$

$$= \frac{1}{m_e}\{K_s\ell(\theta_b - \theta_t) + K_{vs}\ell(\dot{\theta}_b - \dot{\theta}_t) - F_c\}$$

$$y_{tw} = y_s + \ell\sin\theta_b - \Delta y_t$$

$$\dot{y}_{tw} = \dot{y}_s + \ell\dot{\theta}_b\cos\theta_b - \Delta\dot{y}_t$$

contact force

$$F_c = \begin{cases} K_c(y_{tw} - y_o) + K_{vc}(\dot{y}_{tw} - \dot{y}_o) & (y_{tw} - y_o) > 0 \\ 0 & (y_{tw} - y_o) < 0 \end{cases}$$

OHL

$$\ddot{y}_o = \frac{1}{m_o}\{F_c + F_o - K_o y_o - K_{vo}\dot{y}_o\}$$

where:

n = gearbox + belt ratio
J_m = motor inertia
ρ = gearbox efficiency
K_ϕ = torque constant
R = motor winding resistance
K_s = sensor stiffness
K_c, K_{vc} = stiffness and velocity coefficients of contact
K_o, K_{vo} = stiffness and velocity coefficients of OHL
m_e is the effective (cantilever) mass of the brass bar.

Fig. 9 compares the simulated and measured responses.

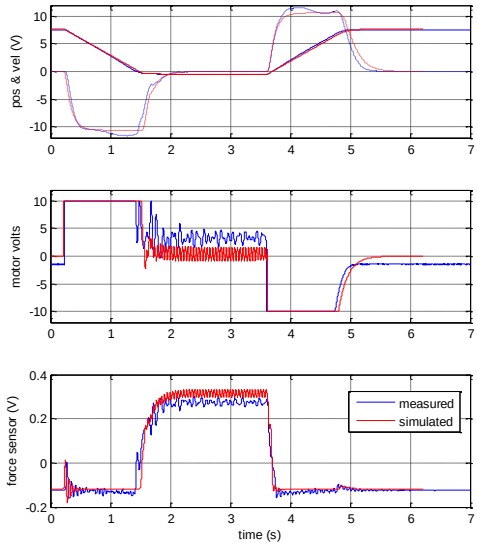

Fig. 9 Simulated and measured responses showing deployment, contact with the OHL and retraction. Values of B = 0.82, $\dot{\theta}_o = 0.56\pi$, F_c = 0.27N and m/M = 75 were used, which are very close to the prototype values.

In Fig. 9, there is excellent agreement between the link position and velocity responses but note that the deployment time is longer than expected because the motor voltage limits. The long time constant of the approximate derivative is also apparent in both the velocity and force signals – this was reduced substantially during later tests. During contact with the OHL, the force signal has a small high frequency oscillation superimposed. This is due to interaction between the OHL and the force sensor which, when fitted with the contact rod, has a prominent resonance at 16Hz. During contact, the measured motor voltage is higher than in the simulation because of the need to overcome static friction in the gearbox.

V. Real-time hardware testing

The experimental pick-up mechanism was mounted under the AVS pod. This was 'flown' at constant speed and height above the OHL while executing a trapezoidal profile in lateral displacement. The real-time controller used the same block diagram as the off-line simulation but embedded into Simulink with ADC/DAC and digital I/O interfaces and then compiled as an executable using Real-Time Workshop. It was found necessary to halve the effective value of the ratio (m/M) in order to obtain a stable response.

Fig. 10 shows a typical result. Both links of the pick-up are initially retracted (at ±90°). At t ~ 62s they drive in at a constant rate until contact is made with the conductors, at which point the force jumps to 0.5 – 0.6N. At t ~ 68s, the AVS pod begins to move along the OHL at about 0.15m/s while executing a trapezoidal lateral displacement profile of ±0.1m amplitude. At t ~ 102s, the pick-up links are retracted.

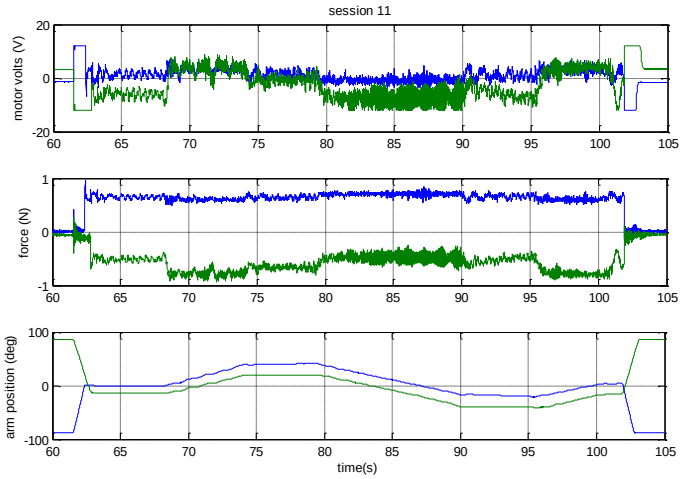

Fig. 10 Result from an AVS test showing the servomotor voltages, sensor forces and link positions.

The angular compensation of the pick-up arms for the pod motion is clearly seen in the bottom graph while the centre graph shows that the contact force remains substantially constant. Again there is substantial noise on the force signals. Fig. 11 is a photograph of the pick-up mechanism in action.

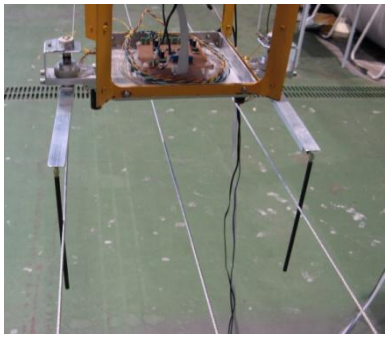

Fig. 11 The pick-up mechanism during contact with the OHL.

VI. Conclusions

This work has shown how a firm sliding contact can be maintained between a pick-up mechanism and the conductors on an OHL using active control. The principal difficulties encountered were: (i) contact between the rod and the OHL caused torsion on the sensor bar that made it twist and also forced it up nearer to the magnetic sensor, (ii) the characteristic of the force sensor varied because the construction of the tip was not sufficiently robust and (iii) oscillation due to the interaction between the OHL and the sensor.

Further work will include a more robust force sensor and control system and integrating the models for the pick-up mechanism and rotorcraft, so that interaction between the two can be predicted. The nature of the electrical contact and the problem of transforming from 11KV to a practical battery voltage will also be addressed.

Acknowledgment

This work was part funded by a Global Research Award from the Royal Academy of Engineering. Thanks are due to Leslie Overs, John Whitham, Steve Nuske and Polly Alexander at CSIRO, Queensland, Australia, for their advice and assistance.

References

[1] C.C. Whitworth, D.I. Jones, A.W.G. Duller and G.K. Earp, "Aerial video inspection of power lines", Power Engineering Journal, vol. 15(1), pp. 25-32, 2001.

[2] G.K. Earp, "Condition Based Risk Assessment of electricity towers using high resolution images from a helicopter", Proc 18th International Conference & Exhibition on Electricity Distribution (CIRED 2005), 2005, Turin, Italy, pp. Paper 610.

[3] C. Sun, R. Jones, H. Talbot, X. Wu, K. Cheong, R. Beare, M. Buckley and M. Berman, "Measuring the distance of vegetation from powerlines using stereo vision", ISPRS Journal of Photogrammetry and Remote Sensing, vol. 60(4), pp. 269-283, 2006.

[4] I.T. Golightly, D.I. Jones, "Visual control of an unmanned aerial vehicle for power line inspection", Proc. IEEE Conf Advanced Robotics (ICAR 2005), 2005, Seattle, USA, pp. 288-295.

[5] J.J. Craig, Introduction to Robotics, 2nd ed, Addison Wesley, 1989.

[6] K. Usher, G. Winstanley, P.I. Corke, D. Stauffacher and R. Carnie, "Air vehicle simulator: an application for a cable array robot", Proc. IEEE Conference on Robotics and Automation, 2005, Barcelona, Spain,, pp. 2253-2258.

[7] N. Hogan, "Stable execution of contact tasks using impedance control", IEEE Int Conf Robotics & Automation, 1987, Raleigh, USA, pp. 1047-1054.